

1 Do sun spots influence the onset of ENSO and PDO events in the Pacific Ocean?

2
3 *Franklin Isaac Ormaza-González¹, and María Esther Espinoza-Celi¹*

4 1) ESPOL Polytechnic University, Escuela Superior Politécnica del Litoral, ESPOL, (Facultad de
5 Ingeniería Marítima, Ciencias Biológicas, Oceánicas y Recursos Naturales), Campus Gustavo
6 Galindo Km. 30.5 Vía Perimetral, P.O. Box 09-01-5863, Guayaquil, Ecuador

7 Corresponding author: formaza@espol.edu.ec.

8 The sea surface temperature (SST), SST anomalies, ONI (Oceanographic El Niño Index) and MEI
9 (Multivariate ENSO Index) in regions El Niño 1+2 (80°W-90°W, 0°-10°S) and 3.4 (5°N-5°S, 170°W-
10 120°W) as well as the Pacific Decadal Oscillation (PDO) and Atlantic Multidecadal Oscillation (AMO)
11 indexes, were correlated to sun spots number (SS) from cycles (SS#) 19 to 24 (1954-2017).
12 Polynomial regression functions represented each of the six cycles with an average $r^2 > 0.89$
13 ($p < 0.001$). Series of correlations between SS and chosen indices at different lag times (0, 6, 12, 24,
14 36 and 48 months) gave a response time of between 12 and 36 months. Over the entire 1954-2017
15 period, the SS cycles did not show a strong correlation with the variables or SST Anomaly in the El
16 Niño areas 1+2 and 3.4. It seems that high and low SS balanced through the cycles. Improved
17 correlations were found for the shorter period 1990-2016. The SST correlations against individual SS
18 cycles in regions 3.4 and 1+2 were up to 0.219 (SS#23) and < 0.0675 (SS#19) correspondingly. SST
19 Anomaly, ONI and MEI correlated with r^2 of 0.250, 0.3943 and 0.2510, one-to-one; the lag time was
20 24-48 months and linear curves had positive slope. In general, more inconsistent and lower
21 correlations were found in 1+2 than in 3.4. On longer time scale indexes, the PDO (as well as the
22 AMO) seemed to respond in 36-48 months to SS cycles (r^2 of 0.625, SS#19) and 0.766, SS#24); whilst
23 the AMO index gave a slightly lower correlation (0.490, SS# 20) with a similar lag time. Further
24 analysis of SS numbers and the oceanic indices above during the ascending and descending phases
25 of each cycle showed SST was best correlated with the ascending phase (up to r^2 of 0.870, with a lag
26 time between SS cycle and index of about 36 months) and this trend also applied to the SST
27 anomaly, although with slightly poorer correlations. The highest r^2 values coincided with strong
28 ENSO events. The descending phase showed lower correlations between SS and ocean indices
29 including MEI and ONI. The PDO was linearly correlated to SS (r^2 0.7677 to 0.2855 (12 to 24 months)
30 as was the AMO (r^2 up to 0.700) whilst during descending phases correlations were poorer. The SS
31 activity seemed to have a better correlation during the cold phase of PDO. AMO and PDO proved to
32 be correlated to SS, with the PDO having a higher correlation. Presumably, as the North Pacific
33 Ocean basin has a larger area than the North Atlantic. The ascending and descending phases of SS
34 could re-inforce or weaken these indexes. The regression linear curves for ascending and descending
35 phases, shows high tendency that ONI, MEI and PDO being negative when SS number are in the
36 range 0-50, whilst the highest positive values are somewhere between 100-200 sun spots per
37 month. These results show that warm events tend to occur in the ascending phase, or at the top of
38 the cycle (as solar radiation increases), and have a delay time of around 24-36 months, whilst cold
39 events are associated with descending phases but with a shorter lag time, 12 months. The
40 correlation analysis given here indicates sun spot activity should be considered as a factor that could
41 condition and trigger low (PDO and AMO) and high (ONI-El Niño) frequency oceanographic events in
42 the Pacific and Atlantic Oceans.

43
44
45 **Key words:** Sun spots cycles, SST, SSTA, ONI, MEI, PDO, AMO, El Niño, La Niña

48 **Introduction.**

49 Essentially, the only external source of energy to Earth is the sun, which constantly radiates a flux of
50 energy to the upper atmosphere (the solar constant) of 1360 W m^{-2} or $1.36 \text{ kJ m}^{-2} \text{ s}^{-1}$ (Monteith,
51 1972) or 1.92 ly day^{-1} (Ormaza-González and Sanchez, 1983). Recently, Kopp and Lean (2011) have
52 reported that the most accurate accepted solar constant value is $1360.8 \pm 0.5 \text{ W m}^{-2}$. Of this flux of
53 energy, 75-50 % reaches the Earth's surface (Ormaza-González and Sanchez, 1983; Lindsey, 2009)
54 and the remainder is reflected and/or absorbed by clouds, particles, gases, etc. (Horning et al.,
55 2003). About 90-93% of that energy reaching the surface is accumulated in the oceans (Trenberth et
56 al., 2014; Clutz, 2017). The solar constant is affected by variations in sun spot (SS) number (Bhowmik
57 and Nandy, 2018) and other solar activity parameters by around 0.1%, i.e. on the order of 1.361 W
58 m^{-2} . The Hale cycle (around 11 years) is characterized by increasing and then decreasing SS numbers
59 (Hathaway, 2015). Froelich (2013) suggested that the solar constant can vary by up to 4.0 W m^{-2} over
60 two SS cycles, i.e. a 22-year cycle, and proposed a simple relationship between SS and the solar
61 constant (SI), by assuming a direct relationship between the two

62 $SI = 1353.6 + 0.089 (SS)$ (r² of 0.71, 95-99% confidence).

63

64 The surface-subsurface layers of the ocean that interact with the lower atmosphere alternately
65 release and absorb heat energy. The work of Zhou and Tung (2010) reported the impact of the SI on
66 global SST over 150 years, finding signals of cooling and warming SSTs at the valley and peak of the
67 SS cycles. Schlesinger and Ramankutty (1994) reported a global cycle of 65-70 years that is possibly
68 affected by greenhouse anthropogenic gases, sulphate aerosols and/or El Niño events, but they did
69 not imply an external force such as the SS. There are well known oceanic events that are roughly
70 periodic with low (25-30 years) or high (3-5 years) frequencies. These include the Pacific Decadal
71 Oscillation (PDO, Mantua et al., 1997; Mantua and Hare, 2002; Zhang et al., 1997; Yim et al., 2013),
72 Atlantic Multidecadal Oscillation (AMO, Enfield et al., 2001; Condrón et al., 2005; Gray et al., 2010)
73 and Interdecadal Pacific Oscillation (IPO, Henley et al., 2015), as well as El Niño (Busalacchi et al.,

74 1983, see **COAPS Library's:** <http://www.coaps.fsu.edu/lib/biblio/coaps-a.html>) or La Niña (Yuan
75 and Yan, 2012). During El Niño events, the surface and subsurface lose energy to the atmosphere
76 and the opposite occurs during La Niña (Trenberth et al. 2014, Fasullo and Nerem, 2016); these
77 events have a periodicity of 2-7 years while the decadal processes may take 25-30 years. The
78 Interdecadal oscillations have a series of impacts; e.g., the PDO gives rise to teleconnections
79 between the tropic and mid-latitudes (Yoon and Yeh, 2010), and the effects include: 1) the ocean
80 heat content (Wang et al., 2017), 2) the lower and higher levels of the trophic chain and small
81 pelagic fisheries including tuna and sardines (Ormaza et al., 2016a, 2016b), 3) biogeochemical air-sea
82 CO₂ fluxes (McKinley et al., 2006), 4) the frequency of la Niña/El Niño (Newman et al. 2003). The
83 interactions between decadal oscillations PDO/IPO and AMO may affect also ocean heat content
84 (Chen and Tung, 2014). All these low and high frequency oceanographic events have a direct impact
85 on local, regional and global climate patterns, and there is growing evidence that the driving source
86 of energy is the sun (Grey et al., 2010). Thus, Huo and Xiao (2016) have found a positive strong
87 correlation between El Niño 2015-2016 and SS, as well as SS and the El Niño Modoki index. White et
88 al., (1997) reported that heat anomalies produced by variable solar irradiance are stored in the
89 upper ocean layer, driving SST changes of 0.01-0.03 K and 0.02-0.05 K on decadal and interdecadal
90 periods respectively. Zong et al. (2014) in their review of the impact of the 11-year SS cycle and
91 multidecadal climate projections, have found global SST variations of 0.08 ± 0.06 K and 0.14 ± 0.02
92 during the 11 and 22 year Hale Cycle, combined with a response lag of 1-2 years in relation to the SS
93 (see also, Kristoufek, 2017). Liu et al. (2015) have reported that effective solar radiation plays a role
94 in the modulation of decadal ENSO (El Niño and the Southern Oscillation) oscillation. More recently,
95 Yamakawa et al. (2016) have reported that solar activities in terms of SS numbers not only affect the
96 troposphere but also the sea surface, even though SS abundance is only a partial measure of solar
97 activity (Scafetta, 2014). The work reported here investigates how sun spots may affect low and
98 high frequency oceanic events such as the Pacific Interdecadal Oscillation (PDO), the Atlantic

99 multidecadal oscillation (AMO), anomalous sea surface temperatures, and El Niño and La Niña
100 events.

101

102 **Material and methods.**

103 Data for monthly sun spot number (SS) were taken from the Royal Observatory of Belgium, Brussels,
104 World Data Center SILSO (<http://www.sidc.be/silso/datafiles>). Data sources for other variables were
105 as follow: El Niño regions areas 3.4 (5°North-5°S, 170-120°W) and 1+2 (0-10°S, 90°W-80°W):

- 106 • **Sea surface temperatures (SST) and SST Anomaly:** The Monthly Extended Reconstructed
107 Sea Surface Temperature Version 4 (ERSSTv4, 1981-2010 base period). The Optimum
108 Interpolation 1/4 Degree Daily Sea Surface Temperature (OISST.v2, 1981-2010 base period),
109 <http://www.cpc.ncep.noaa.gov/data/indices/>.
- 110 • **Oceanic Niño Index (ONI:** Huang et al., 2014): ERSST.v4 for El Niño/La Niña events since
111 1950 till December 2017:
112 http://www.cpc.ncep.noaa.gov/products/analysis_monitoring/ensostuff/ensoyears.shtml.
- 113 • **Multivariate ENSO index (MEI:** Wolter and Timlin, 2011):
114 <https://www.esrl.noaa.gov/psd/enso/mei/table.html>.
- 115 • **Pacific Decadal Oscillation (PDO,** based on Mantua Index): The PDO index is based on
116 NOAA's extended reconstruction of SSTs (ERSST Version 4). It is constructed by regressing
117 the ERSST Anomaly against the Mantua PDO index for their overlap period, to compute a
118 PDO regression map for the North Pacific ERSST Anomaly. The ERSST Anomaly are then
119 projected onto that map to compute the NCEI index. The PDO index closely follows the
120 Mantua PDO index at: <https://www.ncdc.noaa.gov/teleconnections/pdo/> (Wolter and Timlin
121 1993, 1998 and 2011).
- 122 • **Atlantic Multidecadal Oscillation index:**
123 <https://www.esrl.noaa.gov/psd/data/timeseries/AMO/>.

124 All indexes have data from April 1954 to December 2017. The analysis was done using Excel
125 and/or R statistical tools. The correlation exercises were executed using SS solar cycles as
126 complete time series against SST Anomaly (in El Niño regions 3.4 and 1+2), ONI, MEI, AMO and
127 PDO indexes. Correlations with lags of 0 to 48 months were carried out. For the SS cycles 19-23
128 and their impact on the above mentioned dependent variables, correlations were carried out for
129 the whole time series (1954-2017), and for 1990-2016, for each cycle and for their respective
130 ascending and descending phases. Spectral analysis and polynomial regression fitting curves
131 were determined to obtain the slope of the ascending phases; the slopes were correlated to the
132 oceanographic indexes.

133 **Results and discussion:**

134

135 The time series (1954 to 2016) of SS, PDO, AMO, ONI and MEI are shown in Fig. 1. The PDO, AMO,
136 ONI and MEI cycles have been offset by 0, 12, 24 and 36 months (panels a, b, c and d respectively),
137 whilst the SS series starts at t=0 in the four panels. It has been reported that the lag times for
138 responses of some indexes to SS cycles (SS#) are around 12-36 months (e.g., Zhao et al., 2014). From
139 1954 to the present time each cycle 19 to 24 has occurred with a period of around 11 years
140 (Hathaway, 2015), which is slightly less than the 11.2 years reported by Dicker (1978). The highest SS
141 activity is seen in cycle 19 with around 250 SS/month, followed by <150, and at cycle 21 around 200,
142 before decreasing steadily over cycles 22 to 24 to just over 100 SS/month. Cycle 24 is the lowest
143 contemporary value of SS activity that is comparable only to cycles 12-15 (around 1880-1930) and is
144 the lowest in the last 200 years (Clette et al., 2014). The negative or cold PDO phases (1947-1976,
145 2000-June/2016) are within SS cycles 19-20 and 23-24, whilst cycles 21 and 22 are within the
146 positive or warm phase of the PDO (1977-1999). As the PDO and AMO indexes are displaced from 0
147 to 36 months on the time scale (Fig. 1), some peaks and troughs relative to SS activity can be seen.
148 These are at ascending and descending parts of the SS cycles, e.g. during cycles 19-20 and 23-24 PDO
149 indexes are basically negative, whilst during 21-22 they are more positive; an exception is around
150 1990, where there is a strong negative peak. However, AMO phases seem to be in opposition to and
151 overlapping the SS cycles; a cold phase of AMO was between the 1960s and 1990s, whilst the warm
152 phase is from the 1990s to the present (McCarthy and Haigh, 2015).

153

154 The ONI and MEI curves, both indicators of ENSO events, behave similarly throughout the study
155 period (April 1954 – December 2017). However, MEI has the highest anomaly peaks (> 2) when
156 compared to ONI. In general, ONI and MEI curves indicate the highest positive anomalies between
157 1978 and 1995, a period that coincides with the warm and cold phases of PDO and AMO respectively
158 (see Maleski and Martinez, 2018). The opposite trend occurs before and after this period due to the

159 inversion of phases. In addition, the highest peaks of both indexes only occur during the ascending
160 and descending phases of the solar cycles; that is, they never coincide directly with the maximum
161 period of sunspots in the cycles, except in 1959. The two highest MEI peaks occur during the
162 descending phase of solar cycle 21 and ascending phase of solar cycle 23. In mid-2016 both indexes
163 increased reaching the third highest peak of this period during the descending phase of
164 SS#24. Negative peaks of these indexes occurred either in the high or low plateaus of the SS curves.

165

166 The number (N) of data in the analysis were: 765 (1965-2017); 312 (1990-2016); 108 (1990-1999);
167 192 (2000-2016). For individual cycles 19 to 24: 127, 141, 124, 117, 141 and 120 respectively. In the
168 same order for ascending-descending phases: 48-80, 50-92, 43-82, 33-85, 51-51 and 74-47. The
169 degrees of freedom of residuals were N-2. The degree of correlation in terms of Pearson coefficient
170 is referred to as: high, moderate and low when the coefficient is between ± 0.5 and ± 1.0 , ± 0.3 to
171 ± 0.49 and less than ± 0.29 respectively ([http://www.statisticssolutions.com/pearsons-correlation-](http://www.statisticssolutions.com/pearsons-correlation-coefficient/)
172 [coefficient/](http://www.statisticssolutions.com/pearsons-correlation-coefficient/)). All linear regression residuals were auto correlated using the Durbin-Watson (DW) test
173 (Montgomery et al., 2001) for 1954-2017, 1990-2016, 1990-1999, 2000-2016, individual cycles, and
174 ascending-descending phases. The DW test results for the long time series averaged 0.122, for
175 individual cycles it varied from 0.10 to 0.63 with an average of 0.18, and for the ascending and
176 descending phases it averaged 0.40 and varied from 0.1 to 2.24. The SST Anomaly in region ENSO
177 1+2 has the lowest and PDO the highest. Every given caveat associated with correlations was taking
178 into consideration.

179

180 **Whole series (1954-2017) correlations.** All variables (Table 1) were correlated on a linear and
181 polynomial (n= 2 to 6th order) basis using different lag times (0, 6, 12, 24 and 48 months) over the
182 six SS cycles. Polynomial correlation (not shown) as well as linear ones displayed poor correlation
183 coefficients, with the highest linear r^2 ($p \leq 0.01$) coefficients occurring at lag times between 12 and 24

184 months, and 36-48 months for the AMO. For SST and SST Anomaly in ENSO areas 1+2 there was no
185 correlation. These results are like those of Kristoufek (2017), who suggested a surface thermal
186 response of around 24-36 months. The highest correlation r^2 values with SS were up to: 0.043, 0.029,
187 0.040 and 0.021 for PDO, MEI, ONI and SST Anomaly (in 3.4) respectively, indicating there is a
188 correlation with high confidence (p -value ≤ 0.01), though small r^2 . This fact could reflect sun activity
189 (sun spots) in the long term being balanced by the ups and downs of the cycles. This exercise
190 suggests there is not a high correlation of these indexes in the Pacific and Atlantic over the studied
191 time scale. Nonetheless, on longer time scales, where SS cycles are affected by other sun internal
192 processes, e.g., the hypothesized Minimum of Maunder (Eddy, 1976, Shindell et al., 2001, Ineson et
193 al., 2015, Mörner, 2015, etc.), there can be an impact on a global and regional basis. Recently,
194 Lockwood (2010 and 2013) has reported that a grand solar minimum is coming as the SS cycle 24 is
195 developing. There has not been a solar activity decline such as that found in SS# 23 to 24 over the
196 last 9300 years, and such a solar minimum may last through cycles 24, 25 and 26 (Hady, 2013).
197 Under these circumstances where anomalous conditions appear to be developing, it was decided to
198 analyze correlations using individual cycles in the range 19 to 24.

199

200 **Period 1990-2016.** Further analysis was carried out for the period 1990 to 2016, that includes cycles
201 22, 23 and 24. The time series was also split into 1990-1999 and 2000-2016, because during 1990-
202 1999 a strong (1991-1992), moderate (1994-1995) and the strongest El Niño (1997-1998) of the
203 twentieth century occurred. On the other hand, in 2000-2016 (cold phase PDO) there were strong La
204 Niña events (2000-2002 and 2010-2012) and an El Niño Modoki event in 2015 (Huo and Xiao, 2016).
205 Figure 2 shows again a poor correlation (< 0.011 , $p > 0.246$), for the SST Anomaly in region 1+2 (blue
206 bars), although this region was gravely affected by the strong El Niño in 1997-1998 which brought
207 hundreds of casualties and losses of billions of US dollars to the Ecuadorian infrastructure (Glantz,
208 2001). The linear correlation r^2 of SST in 3.4 (red bars) was around 0.1193 ($p \leq 0.00001$) over the

209 whole period, whilst it was somewhat higher in the period 1990-1999 (0.1519, $p \leq 0.01$). The ONI
210 (green bars) correlation coefficient was up to 0.1436 ($p \leq 0.02$) when compared to SS in the period
211 1990-2000, where high positive SST anomalies were present for almost 6 years, and the ONI
212 correlated better than SST anomaly with SS in 3.4. The Pacific Decadal Oscillation (Fig. 2., grey bars)
213 had an r^2 of 0.276 ($p < 0.0001$), in the period 2000-2016 (PDO in a cold phase), with a Pearson
214 correlation of 0.523 that can be considered as high ([https://www.statisticssolutions.com/pearsons-
215 correlation-coefficient/](https://www.statisticssolutions.com/pearsons-correlation-coefficient/)). However, for the period 1990-1999 it was 0.239 and for the whole period
216 was 0.402; i.e. a poor and fair degree of correlation respectively.

217

218 **Individual Cycles.** Correlation analysis was split into SS cycles from 19 to 24. The SS and SST r^2
219 coefficients indicated a poor correlation and confidence level ($p \geq 0.05$) in region 1+2 in all cycles (Fig.
220 3); most of the correlation r^2 values were < 0.050 , except in cycle 19, (r^2 of 0.0675, $p = 0.0032$); in
221 cycles 21 and 23 the highest r^2 was 0.046 ($p = 0.0173$) and 0.048 ($p = 0.037$) respectively. In general,
222 the lag time varied between 6 to 36 months in region 3.4, whose correlations r^2 were up to 0.219
223 ($p \leq 0.0001$) and 0.213 ($p \leq 0.0001$) for cycles 23 and 19 respectively with a lag time of 12-36 months.
224 Cycles 20 and 22 had r^2 of 0.105 ($p \leq 0.0001$) and 0.074 ($p = 0.003$) respectively. The slopes of the
225 linear regression curves with the highest r^2 were positive in region 3.4, indicating a direct correlation
226 between SST and SS cycles. However, cycles 22 and 23 in the region 1+2 exhibited inverse
227 correlation (Fig. 3). Further polynomial correlation ($n = 2$ to 6) analysis did not provide a better r^2 .
228 Over all, higher correlations were found in El Niño regions 3.4 than in 1+2.

229

230 **Anomalies in SST.** The magnitude of the SST Anomaly can change depending on the reference used;
231 there are 5 versions of ERRS (Huang et al., 2017). Currently version 5 tends to be used in El Niño
232 studies. Here we used the ERRSv4 (Huang et al., 2014); Huang et al. (2017) stated that there is not a
233 noticeable difference between ERRSv4 and ERRSv5. The anomalies of SST in 3.4 and 1+2 were also

234 correlated against every SS cycle; correlation r^2 values were not better than 0.396 ($p \leq 0.0001$) in both
235 regions, with higher variability in 1+2 than 3.4 both in response time and correlation coefficient (Fig.
236 4). In region 3.4, the highest correlations were 0.289 ($p \leq 0.0001$) and 0.270 ($p \leq 0.0001$) during cycles
237 19 and 23 respectively, with a lag time of between 12 and 36 months, with both occurring during
238 cold phases of PDO (1955-1978, and 2000-present). Surface winds plus other oceanographic
239 variables (e.g. upwelling) could play an important role in this high variability. Winds are not only
240 generated in the local area but farther away, including the trade winds of the western Atlantic
241 (Ormaza-González and Cedeño, 2017). Also, ENSO processes in the western Pacific could add
242 variability in the SST Anomaly. The slopes of the linear correlation were basically positive for 3.4 and
243 negative for 1+2, and for SST correlations for cycles 19, 23 and 24 (cold PDO phase) had the highest
244 r^2 . Again, the anomalies in 3.4 were better correlated than in region 1+2.

245

246 **ONI.** The El Niño index (Fig. 5) displayed r^2 values when correlated with SS activity from around
247 0.053 ($p=0.01$, SS#22) up to 0.25 ($p << 0.0001$, SS#24); there were poor to fair correlations with a
248 positive slope in SS cycles 19, 23 and 24. During SS#24, ONI reached extreme values of 2.6C (Nov-
249 Dec-Jan 2015/2016) and -1.7C (Oct-Nov-Dec 2010). The highest r^2 were again found with a 24-48
250 months lag time. Cycle 21 did not show any significant correlation with ONI; however, cycles 20, 22
251 and 24 had r^2 values of 0.144 ($p << 0.001$), 0.131 ($p << 0.0001$) and 0.252 ($p << 0.0001$) and lag times of
252 48, 12, and 24 months respectively. Recently, Huo and Xiao (2016) found strong correlation between
253 SS and El Niño Modoki during 2015 (SS#24). The variability in correlations could arise from: 1) SS
254 numbers showing large variations from one month to another, 2) regional meteorological conditions
255 (particularly cloudiness), ocean surface currents that exchanges heat in region 3.4, 3) Kelvin waves
256 (Gill, 1982), 4) the Southern Oscillation Index (SOI: Southern Oscillation Index:
257 <http://www.cpc.ncep.noaa.gov/data/indices/soi>). All these may affect the SSTs and together with
258 the way ONI is obtained, as the ONI has a variable reference period of 30 years; thus for 1950 to

259 1955 the reference period is 1936-1965; for 1956-1960; 1941-1970. The ERRSv4 uses the period
260 1981-2010. The reference period is changed every 5 years (Lindsey, 2013); the most recent ONIs
261 (v4/v5) are supposed to use better and more consistent information as data acquisition improves.

262

263 **MEI.** This additional index for El Niño events had a lower correlation (r^2) with SS; thus, the highest
264 value was 0.3943 ($p < 0.00101$, SS#19), the next 0.3028 ($p < 0.00001$, SS#24), 0.2421 ($p < 0.00001$,
265 SS#23) and 0.1566 ($p < 0.0001$, SS#20); in cycles 21 and 22 no correlation better than 0.1232
266 ($p < 0.0001$) was found. The lag time for sun spot activity (with the highest correlations) ranges from
267 24-48 months; and linear regression curves were with mainly positive slopes. The lower correlation
268 found could be explained as this index comprehend six variables, and some of these could not be
269 directly or are weakly related to SS; like zonal and meridional components of surface wind, surface
270 air temperature, cloudiness (Wolter and Timlin, 1993).

271 **PDO.** This interdecadal index (Fig. 5) is linearly correlated to SS cycles with a lag time between 36
272 and 48 months, with the highest r^2 of 0.391 ($p < 0.00001$) in cycle 19, and 0.586 ($p < 0.00001$) for
273 cycle 24. Both cycles are within the cold phase of the PDO. The next highest r^2 with p-values
274 < 0.0001 were 0.218, 0.1361, 0.218 and 0.260 for cycles 20-23. In all cycles, the highest r^2 were
275 directly correlated, except cycle 20. For some reason, there appears a better fit with both PDO and
276 ONI in cycles 19 and 24, which are within the cold phase of the PDO, even though these cycles have
277 remarkably different shapes and peaks (Fig. 10). Cycle 19 registered SS counts of over 250 whilst
278 cycle 24 was just around 100; also, the peaks were different being respectively very sharp and
279 extended. The direct relationship between PDO and ONI has been reported extensively (e.g.
280 Ormaza-Gonzalez et al., 2016a, Jia and Ge, 2017).

281

282 **AMO.** This index gave correlation coefficients (r^2) with SS numbers of up to 0.490 ($p < 0.00001$) and
283 down to 0.162 ($p = 0.0004$) in cycles 20 and 24 respectively, when a lag time of 48 months was used.
284 With cycles 19, 21 and 22 the best fit elapsed time was 24-36 months (Fig. 5). Gray et al. (2016)
285 reported lag time responses of mean-sea-level pressure over the Atlantic to SS cycles of 36-48
286 months over a longer time series study of 32 solar cycles. The linear regression analysis rendered
287 positive and negative slopes for cycles 19, 23 and 24; and 20 to 22, respectively. This coincides with
288 the phases of the AMO, negative from around 1965 to 1998 (SS cycles 20-22), and positive; 1930-
289 1965 (SS cycle 19) and after 1998 (SS cycles 23-24), <http://appinsys.com/globalwarming/amo.htm> . It
290 is noteworthy that the slopes of the PDO and AMO linear regressions are negative and positive
291 respectively for cycles 21 and 22, but in concordance in cycles 19, 20, 23 and 24 (cold phase PDO).

292

293 **Ascending and descending phases** of solar cycles. As the SS cycles are best related to variables
294 studied on a response time from 24 to 36 months, there was the need to study their influence during
295 the ascending and descending phases, which have roughly 5-6 years duration. Polynomial regression
296 analysis was performed to establish a function that could best describe every SS cycle. Sixth-order
297 polynomial curves (Fig. 10) were found to render a very strong correlation coefficient averaging 0.89
298 ($p \leq 0.001$). These functions allowed the analysis of correlations in the ascending and descending
299 phases.

300

301 **SST in 1+2 and 3.4.** In region 1+2, the highest correlation coefficient r^2 were: 0.205 (SS#23), 0.189
302 (SS#21), and 0.163 (SS#19). All linear regression coefficients r^2 over 0.0847 ($p < 0.05$ to $= 0.0008$)
303 occurred in the ascending phase of the SS cycles, whilst those in the descending phase were lower,
304 with no definite lag time pattern from 0 to 36 months. The slope (positive/negative) of the linear
305 regression (Fig. 6) curves showed no pattern. These low and variable r^2 values reflect region 1+2
306 being subjected to the combined impact of many diurnal and seasonal oceanographic and

307 meteorological variables. For example, during the first quarter of 2017 (cycle 24), in 1+2 there was a
308 higher than usual SST because the southern trade winds in the eastern Pacific weakened whilst
309 those in the North Atlantic strengthened. These winds passed through the Panama Isthmus and
310 blew warm (up to 30C) surface waters from the Panama Bay southwards towards area 1+2, thus
311 provoking a rapid and relatively short lived surface warming event (Ormaza-González and Cedeño,
312 2017), whilst region 3.4 was registering La Niña conditions. Even though, this cold event also
313 strengthens the Cromwell Undercurrent (Knauss, 1959) and Humboldt (Montecino and Lange, 2009)
314 currents that impact upwelling processes in 1+2, the surface warm event was not suppressed;
315 Ramírez and Briones (2017) called this event El Niño Costero. All these factors would mask the SS
316 signal in area 1+2. Nonetheless, it could be observed that during the ascending phases of the cycles,
317 the correlation of SSTs was higher than in the descending phase of cycles

318

319 In the region 3.4, the maximum r^2 of SST in each SS cycle was found at a lag time of 36 months with
320 all of them occurring at the ascending phase, except in cycles 20 and 24. The four highest r^2 values
321 were 0.870 ($p=0.021$, SS#24), 0.613 ($p<<0.0001$, SS#22), 0.574 ($p<<0.0001$, SS#19), and 0.556
322 ($p<<0.0001$, SS#23) with Pearson coefficients of 0.9327, 0.7803, 0.7576 and 0.7456, respectively,
323 thus showing a strong degree of linear correlation. Linear regression slopes were variable (Fig. 6),
324 although there was a tendency in cycles 20, 21 and 22 (warm PDO) for negative slopes and for
325 positive slopes for cycles 19, 23 and 24 (cold phase PDO). In area 3.4 the SST response to SS was
326 much clearer than for 1+2, as in this region (10N-10S and 120W-180W) there is no influence of
327 coastal processes. The highest r^2 (0.870, $p=0.021$; lag time 36 months) in the descending phase in
328 cycle 24 coincided with the strongest El Niño, and the second-highest r^2 (0.613, $p<<0.00001$) during
329 ascending phase of cycle 22 with two consecutive strong El Niño 1991-1995; the third r^2 (0.574,
330 $p<<0.00001$) during cycle 19, with el Niño 1955-1957, and finally the fourth r^2 (0.556, $p<<0.00001$)
331 with the 1997-1998 warm event during cycle 23. It seems that over the relatively short time scales of

332 SS cycles, either on their initial ascending or subsequent descending phases, impacts on the SSTs can
333 be triggered.

334

335 **SST Anomaly.** In region 1+2 (Fig. 7), the anomalies registered high r^2 ($p < 0.0001$) of 0.662 (SS#22),
336 0.637 (SS#19), 0.523 (SS#21), 0.480 (SS#23), 0.359 (SS#24); and 0.254 ($p = 0.0002$, SS#20)
337 respectively, in the ascending phase of the SS cycles and with a positive linear regression slope
338 (except SS#23). The response lag time was somewhere between 0 and 48 months. On the other
339 hand, the descending phase showed a predominantly lower r^2 , less than 0.14 with lower significance
340 ($p \leq 0.02$), with the exception in SS# 19, 0.304 ($p < 0.0001$). The results suggest that during cold
341 phase PDOs when Northern Pacific basin surface ocean waters are relatively colder, the correlations
342 in this area tend to be higher, as the increasing sun radiation augments the heat content (i.e., SST) of
343 the ocean surface.

344

345 In region 3.4, there was a high and consistent r^2 (Fig. 7) that reached up to 0.897 ($p = 0.014$; SS#24);
346 0.863 ($p < 0.0001$; SS#22); 0.665 ($p < 0.0001$; SS#19), 0.826 ($p < 0.0001$; SS#23), then fell to 0.211
347 ($p = 0.008$; SS# 20); 0.239 ($p = 0.0009$; SS# 21) respectively; all of them were in the ascending phase
348 except cycles 20 and 24. The lag time was consistent at 36 months. Linear regression slopes were
349 variable (Fig. 8) with negative slopes in cycles 20-22 (warm phase PDO), and positive slopes in 19, 23
350 and 24 cycles (cold phase PDO). The highest r^2 of 0.897 at the start of the descending phase in 24
351 coincided with one of the strongest El Niño and the second r^2 (SS#22 ascending phase) with two
352 consecutive strong El Niño 1991-1995. The third and fourth highest r^2 were during El Niño 1955-1957
353 and 1997-1998 warm event (SS#23 ascending) respectively. The results suggest that SS cycles are
354 strongly correlated to SST Anomalies in both El Niño regions, with the strongest relationship in 3.4.

355

356 **The ONI index.** This index as well as SST and its anomalies in 3.4, were equally strongly associated
357 with the ascending phase of the SS cycles (Fig. 8), with lag times of 24-36 months. The highest
358 correlation r^2 for each cycle were in the ascending phase, the predominant linear regression slopes
359 were positive, except for SS#20. The highest r^2 ($p < 0.0001$) were: 0.817 (SS#22), 0.693 (SS#19),
360 0.637 (SS#23), 0.3547 (SS#24), 0.2876 (SS#20); 0.1936 ($p = 0.003$, SS#21). The three highest r^2 match
361 the dates of full-fledged strong El Niño 1955-1957, 1987-1989, and 1997-1998 (Fig. 9) with positive
362 slopes on the ascending phase. In the descending phase the r^2 ($p < 0.0001$) in cycles 24, 23, 22 and
363 20 were 0.366, 0.284, 0.255, and 0.242 respectively. All had a lag time 0-12 months and positive
364 slopes. Cycles 19 and 21 showed neither strong correlation (< 0.1) or confidence values ($p = 0.2$). The
365 ONI correlations are in accordance to what found with SST anomalies in 3.4.

366

367 Warm events tend to occur in both ascending/descending phases after the peak/trough, and have a
368 delay time of 24-36 months, which is similar to findings of Huo and Xiao (2016). The delay time, is
369 probably due to the slow accumulation of solar heat over time in surface oceanic waters. The
370 descending phase of the cycles (Fig. 8), with a generally smaller slope than the ascending phase,
371 produces a quicker response (0-12 months) to the ocean surface SST and ONI that could trigger
372 neutral or cold events more cogently. Most of the La Niña events occur during the descending phase
373 or approaching the cycle minimum (Fig. 10), when the solar irradiance (SI) decreases slightly as does
374 the number of sunspots. The weakest sunspot cycle (SS#24) has had three La Niña events: 2007-
375 2009, 2010-2012, 2016-2017 (Fig. 10). A plausible reason is that during this cycle the number of sun
376 spots (i.e. sun activity) is the lowest in the last two centennials (Clette et al., 2014); therefore, less
377 energy has hit the ocean surface allowing a cooling effect. Two important exceptions are La Niña
378 1988-1989 (22) and 2000-2002 (cycle 23) that occurred in the ascending phase.

379

380 **The MEI index.** The Multivariate ENSO Index does not only consider the SST Anomaly but also sea-
381 level pressure (Allan and Ansell, 2006) and other variables. These variables include surface winds
382 (meridional and zonal), surface air temperature and cloudiness (Wolter and Timlin, 1998). The MEI
383 correlated at slightly lower levels than ONI to SS cycles with r^2 : 0.784 ($p \leq 0.0001$), 0.770
384 ($p < 0.0001$), 0.5972 ($p \leq 0.0001$); 0.3396 ($p \leq 0.0001$); 0.2368 ($p = 0.0003$); and 0.222 ($p = 0.001$) for SS
385 cycles 19, 22, 23, 24, 20, and 21, respectively. All of them were in the ascending phase of the cycles
386 with lag times from 12 to 48 months (except cycles 23 and 24), with a positive linear regression
387 slope. Exceptions were 22 and 20 where the r^2 was largest with a zero lag time. During the
388 descending phase, as with the ONI, the r^2 were lower: 0.321 ($p = 0.0004$, SS#24); 0.3145 ($p < 0.0001$,
389 SS#19); 0.2234 ($p < 0.0001$, SS#22); 0.2088 ($p < 0.0001$, SS#20), and 0.1438 ($p = 0.0002$, SS#23) with
390 positive slopes (except SS# 20), and lag times were in a larger 0-48 months range; cycle 21 did not
391 have a r^2 above 0.010 ($p > 0.02$). The much lower r^2 , during descending phases, when there is less sun
392 radiation energy (see formula 1), could lead to La Niña events, which has actually occurred over the
393 six cycles. Also, the lower correlations could be because the MEI uses five variables more than the
394 ONI, and these could thus help obscure the signal from the sun's irradiation.

395

396 **PDO.** The Pacific Decadal oscillation gave positive slope linear correlations with SS in most cycles
397 except cycles 20 and 21 (Fig. 9). Correlation coefficients of 0.7677 ($p \leq 10^{-12}$), 0.6577 ($p \leq 10^{-12}$),
398 0.6734 ($p \leq 10^{-7}$) and 0.5062 ($p \leq 10^{-7}$) for the ascending phase SS#19 (Apr/54-Nov/58), SS#24
399 (Jan/08-Feb/14), SS#22 (Sep/86-Jan/89) and SS#23 (May/90-Jun/00) respectively were found. All
400 these coefficients were obtained at a lag time of 12-48 months, except 22 and 23 (lag time = 0). The
401 slopes of the linear regressions were mainly positive during cold phase PDOs (cycles 19, 23 and 24),
402 except cycle 20 when a cold PDO was transitioning to a warm PDO (cycles 21 and 22). The two
403 highest r^2 values are at a lag time of 12-36 months, for cycles 19 and 24, as has been reported (e.g.,
404 Huo and Xiao, 2017). During the descending phase, the correlation r^2 tended to be much lower, with

405 the highest 0.3522 ($p < 0.00001$) and 0.3452 ($p < 0.00001$) at cycles 19 and 20. Sun spot energy
406 variations on long time scales (van Loon et al. 2007), even with very weak changes, could produce
407 decadal and millennial timescale impacts on global thermohaline circulation that in turn affect heat
408 distribution (Bond et al. 2001, Gray et al., 2013).

409

410 **AMO.** The correlations were generally higher at the descending phase of the SS cycles, which is
411 opposite to those for SS vs PDO, ONI, MEI, and the SST Anomaly. However, the highest r^2 occurred
412 on ascending (A) and descending (D) phases of SS cycles, thus: 0.700 ($p < 10^{-10}$), 0.558 ($p < 10^{-10}$),
413 0.468 ($p < 10^{-10}$), 0.434 ($p = 0.03$), 0.411 ($p < 0.00001$) and 0.191 ($p = 0.001$) for cycles 20A, 22D, 19D,
414 24D, 21A and 23A, respectively. These high r^2 values show a strong degree of correlation, although
415 lower than PDO correlations. The lag time was between 24-48 months. The results found could be
416 explained as The Atlantic Multidecadal Oscillation index has the opposite phase to the PDO (Enfield
417 et al., 2001; Condrón et al., 2005); i.e. warm in periods 1930-1964 and 2000-present (cold PDO), and
418 cold in 1965-1999 (warm PDO). The PDO and AMO are inter-decadal cycles of 25-30 years, therefore
419 during the ascending and descending phase they strengthen or weakened.

420 **Conclusions**

421

422 **Period 1954-2017.** Over this period sun spot numbers have decreased from between 225 (SS#21)
423 and 110 (SS#24) at cycle maxima, to minima SS counts of around 20-25. Thus, the Earth is receiving
424 decreasing solar energy over this almost 7-decade period. The reduction of SS peaks has been
425 associated with the beginning of the Maunder Minimum (Mörner, 2015). Ineson et al. (2014) are
426 projecting lower peaks for the next SS cycle (SS#25) and presently SS counts per month are as low as
427 1.6 (July 2018) and with an average of 8.5 (Jan-Aug 2018); counts are expected to decrease to 5.3 in
428 February 2019, actually it decreased to 0.8 (<http://www.sws.bom.gov.au/Solar/1/6>).

429 Monthly SS count correlations with SST, SST Anomaly (both 3.4 and 1+2), ONI, MEI, AMO and PDO
430 through the whole time series (1954-2017) were poor; these had a correlation r^2 values averaging
431 0.020 and a negative linear regression slope. Thus, in the long term there are no strong correlations
432 between SS and PDO, MEI, ONI and SST Anomaly in 3.4 (correlation coefficients were between 0.043
433 and 0.021). In the case of region 1+2, the correlation was even poorer: <0.005 .

434

435 The series of correlations at different lag times (6, 12, 24, 36 and 48 months) gave a response time
436 (i.e. the lag time with highest correlation coefficients; Table 1) of 12-24 months for all indexes,
437 except for AMO (48 months), which align to what was previously reported by Kristoufek, (2017), and
438 Huo and Xiao (2016);

439

440 Changes of the SS cycle could have climate impacts. Gil-Alana et al. (2014) have found no significant
441 statistical relation between sun spots and global temperature; however, van Loon et al. (2007)
442 suggested that even though SS cycles produce weak changes on Solar Irradiation (SI) of about 0.07%
443 according to Gray et al. (2010), these can still produce decadal and millennial impacts on global

444 thermohaline circulation (Bond et al. 2001, Gray et al., 2016), due chiefly to UV energy fluctuation
445 (Ineson et al., 2014). The changes in UV (<100 nm to 350 nm) and near infrared (>800 nm to >1000
446 nm) are larger than in the visible range (>350 nm-800 nm) and could have an important impact on
447 global climate (Ermelo et al. 2013). It is therefore reasonable to expect some impact on the studied
448 oceanographic indexes. Recent data (Solar Radiation and Climate Experiment Satellite) suggest that
449 the variability of UV radiation during the declining phase of cycle 23 was larger than previous
450 estimates (Harder et al., 2009 and Haigh et al., 2010). The SI variations are strongly correlated to SS,
451 and even though these are relatively small (Hansen et al., 2013), they may impact surface ocean
452 heat content because: 1) the total SI integrates over all the wavelengths, and 2) the heat capacity of
453 the seawater is huge. Also, UV radiation penetrates down to 75-100 m depth in the water column
454 (Smyth, 2011), thus adding to the heat content of the deeper layers.

455

456 **Individual SS cycles (19-24).** The SST shows some correlations against individual SS cycles in regions
457 3.4 and 1+2. In the first (Fig. 3), these were up to 0.219 (SS#23) whilst the lag time was 12-36 months
458 in all cycles (except SS#19), in line with reports from Kristoufek (2017) and Huo and Xiao (2016). On
459 the other hand, in region 1+2, the linear correlation r^2 was low at <0.0675 (SS#19), and highly
460 inconstant between cycles. The SS and SST anomaly correlations in 3.4 and 1+2 (Fig. 4), showed
461 important variability with highest values of 0.289 (in 3.4) and 0.396 (in 1+2) during cycles 19 and 24
462 respectively, with both having the same response time range. These values are within the cold phase
463 of the PDO, suggesting that during this phase the signal from SS is clearer. In the period 1997-2016
464 the two strongest El Niño (1997-1998 and 2015) and La Niña (2000-2002 and 2010-2012), events
465 occurred, and they were most evident in the 1+2 region. The slopes of the linear correlation were
466 positive for 3.4 and negative for 1+2, and in general it was found that correlations were more
467 inconstant and lower in 1+2 than in 3.4, also the linear regression curves show when SS approaches
468 to zero the value of SST and SST anomaly as well as ONI and MEI, as well as PDO are negative. These

469 results do suggest that Sun spot activity can influence the SST and SST anomaly behavior, but the
470 relatively weak signals may well reflect high seasonal and interannual variability in coastal
471 oceanographic conditions (Ormaza-González and Cedeño, 2017) that obscures the correlation with
472 SS. In zone 3.4, correlations are better, although the influence of regional oceanographic and
473 meteorological conditions will still be there as expressed through, e.g., the Southern Oscillation
474 Index – SOI - (Rasmussen and Carpenter, 1982; Barnston, 2015). The SOI temporal behaviour have
475 also been associated to SS and could enhance or mar the oceanographic indexes of the equatorial
476 Pacific (Higginson et al., 2004). During cycle 24, the ONI index was highly correlated to SS (r^2 up to
477 0.2510) with a positive slope (Fig. 5). The ONI index reached 2.6C (Nov-Dec-Jan 2015/2016) and -
478 1.7C (Oct-Nov-Dec 2010). In cycles 20-21 the r^2 was low ($r^2 < 0.04$); however, from 22 to 24, r^2
479 increased from 0.131 ($p < 0.00006$) to 0.251; thus, confirming the SS activity has a better correlation
480 during the cold phase of PDO.

481

482 The PDO aligned best with SS cycles at lag times of 36-48 months during SS#19 (0.625) and SS#24
483 (0.766) when the PDO was in a cold phase, whilst lower correlations (0.467-0.508 for cycles 20-23)
484 were found when it is in a warm phase (1979-2000) or in between them. The North Atlantic index
485 counterpart (AMO), gave a variable lower correlation r^2 ranged from 0.130 to 0.490 with a response
486 time of 48 months for cycles 23 and 20 respectively. Gray et al. (2016) reported 36-48 months lag for
487 mean-sea-level pressure in the North Atlantic in a study of 32 SS cycles. The slopes of the PDO and
488 AMO linear regression curves are negative and positive respectively in cycle 21 and 22, but in
489 concordance in 19, 20, 23 and 24 during the cold phase of the PDO. These two interdecadal
490 oscillations proved to be correlated to SS, with the PDO having a higher correlation. Presumably, as
491 the North Pacific Ocean basin has a larger area than the North Atlantic the correlations and lag times
492 may reflect the higher heat storage capacity in the North Pacific.

493

494 **Ascending and descending phases.** The SSTs in 1+2 showed higher correlations with SS in the
495 ascending phases, relative to the descending phase (r^2 of up to 0.205 and below 0.067 respectively).
496 In region 3.4, there were again high degrees of correlation of SS and SST (r^2 between 0.87 and 0.56),
497 during the ascending phase of the cycles, with a response time of 24-36 months seems to occur at
498 the low or high plateau of the cycles (Fig. 10). The highest r^2 of 0.870 in the descending phase in
499 cycle 24 coincided with the strongest El Niño (2015) and the second highest (SS#22) with two
500 consecutive strong El Niño events in 1991-1995; the third and fourth highest corresponded with el
501 Niño and warm events respectively in 1955-1957 and 1997-1998. It seems that short time
502 expressions of SS cycles, either at the beginning of their ascending or descending phases, have a
503 trigger effect on the SSTs. This was observed through the polynomial regression curves (Fig. 10) that
504 were found for each SS cycle, as the SI (equation 1) increases and decreases the amount of heating
505 of surface waters follows suit. The polynomial curves (6th order) were fitted with an average $r^2 > 0.89$.
506 Thus, the warm events El Niño of: 1957-1958 (SS# 19), 1965-1966 (SS# 20), 1981-1982 (SS# 21),
507 1987-1988 and 1991-1992 (SS# 22), 1997-1998 (SS# 23), 2015-2016 (SS# 24). On the other hand, the
508 cold events of La Niña tend to occur after an El Niño at the middle of the ascending phases (1988-
509 1989, 1999-2001, 2010-2012) or when approaching the minimum of the cycles (1973-1974, 1975-
510 1975; 1995-1996, 2017-2018). The so called equatorial Pacific neutral conditions in 3.4 (see,
511 https://iridl.ldeo.columbia.edu/maproom/ENSO/ENSO_Info.html), seems to span a longer period
512 after La Niña, and vice versa after El Niño.

513

514 The ENSO indexes ONI and MEI also showed strong correlations to the ascending phase of the SS
515 cycles, with a lag time of 24-36 months. The regression linear curves for ascending and descending
516 phases, shows that these indexes are negative when SS number are in the range 0-50, whilst the
517 highest positive values are somewhere between 150-200 sun spots per month. In this analysis, it was
518 besides found that warm events tend to occur in the ascending phase (SI increases) or at the top of

519 the cycle and have a delay time of 24-36 months (as also reported by Huo and Xiao, 2016), whilst
520 cold events are mostly associated with a descending phase (SI decrease) but with a quicker response
521 time of 0-12 months. The MEI index has a similar pattern to the ONI, but with lower correlations that
522 may arise as the MEI takes into consideration six variables that in combination may mask the signal
523 from sun activity.

524

525 The linear regression curves (Fig. 11) at SS close to zero the ONI is somewhere between 0C to -2C,
526 whilst in the range 50-200 sun spots the ONI is predominantly positive. Over all, for all ascendant
527 phase together gives an r^2 ($p < 0.01$) of 0.11, in some cycles (22 and 23) the r^2 was 0.6. We deem this
528 a clear evidence how SS (read solar radiation) affect the studied indexes.

529

530 The PDO was linearly correlated to SS (r^2 ranging from 0.285 to 0.768) in the ascending phase with
531 lag times of 24-36 months (Huo and Xiao, 2016), whilst correlations with AMO varied with r^2
532 between 0.160 to 0.700. Similarly, the response time was 24-48 months. These results correspond
533 with those of van Loon et al. (2007), who established that even a small change (1.5 W m^{-2}) in sun
534 activity (SI) could produce decadal and millennial time scales influences on thermohaline circulation
535 (Bond et al. 2001, Gray et al., 2016); nonetheless, the Intergovernmental Panel on Climate Change:
536 IPCC (2001) considers this fact too small to drive climate changes. These influences of this change
537 can be reflected by PDO and AMO indexes, which are found to be in the opposite phase to PDO
538 (Enfield et al., 2001; Condrón et al., 2005). The ascending and descending phases of SS could re-
539 inforce or weaken these indexes.

540

541 Recent predictions for an El Niño event in the late northern hemisphere summer of 2018 (see:
542 <http://www.bom.gov.au/climate/enso/>) did not occur; then, projections were pushed back to the

543 beginning of autumn (<http://www.cpc.ncep.noaa.gov/products/precip/CWlink/MJO/enso.shtml>)
544 and most recently late autumn and winter 2019. Thus, most current models are failing to provide a
545 consistent projection. This is likely related to two re-cooling events in all El Niño areas, that have
546 kept the ONI index within the realm of ENSO neutrality (-0.5C to 0.5C). Also, the PDO indexes have
547 been negative, averaging -0.53, and it is now in its cold phase
548 (<https://www.ncdc.noaa.gov/teleconnections/pdo/>). This coincides that during 2017 the average
549 smoothed SS counts per month was 21.8, and for 2018 it was 8.5 with many weeks without any SS.
550 In July the average SS count was just 1.6 (<http://www.sws.bom.gov.au/Solar/1/6>) with counts
551 expected to decrease to 5.3 in February 2019 (actually they were just 0.8). Therefore, the input of
552 solar heat has been at its lowest values since the 1950s, and its trigger effect on ENSO system is not
553 enough for a full-fledge El Niño event; id est, meteorological (SOI) and oceanographic (ONI or MEI)
554 are not connected for around three consecutive months (Australian Bureau of Meteorology,
555 <http://www.bom.gov.au/climate/enso/#tabs=Overview>) . At the time of writing this paper, the
556 expected and modelled 2018 full-fledged El Niño 2018 did not occur, it did not happen, actually the
557 region 3.4 and 1+2 cooled down by the end of 2018. During March 2019, the latest report from
558 <http://www.bom.gov.au/climate/enso/#tabs=Overview> is saying “The El Niño–Southern Oscillation
559 (ENSO) remains neutral. However, the Bureau's *ENSO Outlook* remains at El Niño WATCH, meaning
560 there is approximately a 50% chance of El Niño developing during the southern hemisphere autumn
561 or winter...”. Nonetheless, NOAA view is that a weak El Niño conditions are present now and to
562 expect to continue through the Northern Hemisphere spring 2019 (~55% chance),
563 [https://www.cpc.ncep.noaa.gov/products/analysis_monitoring/lanina/enso_evolution-status-fcsts-](https://www.cpc.ncep.noaa.gov/products/analysis_monitoring/lanina/enso_evolution-status-fcsts-web.pdf)
564 [web.pdf](https://www.cpc.ncep.noaa.gov/products/analysis_monitoring/lanina/enso_evolution-status-fcsts-web.pdf). The fact is, El Niño is not fully-fledged. At this moment (march 24, 2019) the oceanographic
565 and meteorological variables have not fully couple yet. The ENSO modellers should take into
566 account in some way the presence of SS or any variable that could measure the variability of SI as an
567 input to the models, specially the determinists ones.

568

569 **Data availability.** All data are publicly available on the Web (see Material and Methods).

570

571 **Author contributions.** Franklin Isaac Ormaza-González led and oversaw the whole project. He
572 conceptualized the hypothesis, researched the literature, designed the material and methods, and
573 wrote the paper in all its stages. María Esther Espinoza-Celi looked for and retrieved all data and
574 information, run statistical and spectral analysis, organized results, and designed graphs. She
575 designed the poster presentation.

576

577 **Acknowledgements.** Authors are grateful to ESPOL authorities whose supported research allotting
578 time and financial resources to present paper in the “4TH INTERNATIONAL SYMPOSIUM: THE
579 CLIMATE CHANGE EFFECTS ON THE WORLD OCEANS” held in Washington DC, 4-8 June 2018, also
580 The National Chamber of Fisheries of Ecuador support is acknowledged. Work on the English by
581 Dafne Vera-Mosquera and anonymous scientist is indeed appreciated.

582 **References**

- 583 1. Allan, R.J., and Ansell, T.: A new globally complete monthly historical gridded mean sea level
584 pressure dataset (HadSLP2): 1850-2004, *J. Climate*, 19, 5816-5842, 2006.
- 585 2. Barnston, A.: Why are there so many ENSO indexes, instead of just one?
586 [https://www.climate.gov/news-features/blogs/enso/why-are-there-so-many-enso-indexes-
587 instead-just-one](https://www.climate.gov/news-features/blogs/enso/why-are-there-so-many-enso-indexes-
587 instead-just-one) (last access: 15 March 2018), 2015.
- 588 3. Bond, G. G., Kromer, B., Beer, J., Muscheler, R., Evans, M., Showers, W., Hoffmann, S., Lotti-
589 Bond, R., Hajdas, I., and Bonani, G.: Persistent Solar Influence on North Atlantic Climate
590 During the Holocene, *Science*, 294, 2130–2136, 2001.
- 591 4. Bhowmik, P. and Nandy, D.: Prediction of the strength and timing of sunspot cycle 25 reveal
592 decadal-scale space environmental conditions. *NATURE COMMUNICATIONS* (2018) 9:5209.
593 <https://doi.org/10.1038/s41467-018-07690-0>.
- 594 5. Busalacchi, A.J., Takeuchi, K., and O'Brien, J.J.: Interannual variability of the equatorial
595 Pacific-revisited, *J. Geophys. Res.*, 88, 7551-7562, 1983.
- 596 6. Chen, X., and Tung, K.K.: Varying planetary heat sink led to global-warming slowdown and
597 acceleration, *Science*, 345, 897–903, doi:10.1126/science.1254937, 2014.
- 598 7. Clette, F., Svalgaard, L., Vaquero, J. M., and Cliver, E. W.: Revisiting the Sunspot Number,
599 *Space Sci. Rev.*, 186, 35-103, doi: 10.1007/s11214-014-0074-2, 2014.
- 600 8. Clutz, R.: Global ocean cooling in September (2017),
601 <https://rclutz.wordpress.com/2017/10/26/global-ocean-cooling-in-september/> (last access:
602 30 October 2017), 2017.
- 603 9. Compo, G.P., and Sardeshmukh, P.D.: Oceanic influences on recent continental warming,
604 *Clim. Dynam.*, 32, 333-342, doi:10.1007/s00382-008-0448-9, 2009.
- 605 10. Condrón, A., DeConto, R., Bradley, R. S., and Juanes, F.: Multidecadal North Atlantic climate
606 variability and its effect on North American salmon abundance, *J. Geophys. Res. Lett.*,
607 32L23703, doi:10.1029/2005GL024239, 2005.

- 608 11. Dicke, R.H.: Is there a chronometer hidden deep in the Sun? *Nature*, 276, 676-680, 1978.
- 609 12. Eddy, J. A.: The Maunder Minimum, *Science*, 192 (4245), 1189–1202,
610 doi:10.1126/science.192.4245.1189, 1976.
- 611 13. Enfield, D.B., Mestas-Nuñez, A.M., and Trimble, P.J.: The Atlantic multidecadal oscillation
612 and its relation to rainfall and river flows in the continental US, *J. Geophys. Res. Lett.*, 28,
613 2077–2080, doi:10.1029/2000GL012745, 2001.
- 614 14. Ermolli, I., Matthes, K., Dudok de Wit, T., Krivova, N. A., Tourpali, K., Weber, M., Unruh, Y. C.,
615 Gray, L., Langematz, U., Pilewskie, P., Rozanov, E., Schmutz, W., Shapiro, A., Solanki, S. K.,
616 and Woods, T.N.: Recent variability of the solar spectral irradiance and its impact on climate
617 modelling, *Atmos. Chem. Phys.*, 13, 3945-3977, doi:10.5194/acp-13-3945-2013, 2013.
- 618 15. Fasullo, J., and Nerem, R.: Interannual variability in global mean sea level estimated from the
619 CESM Large and last millennium ensembles, *Water*, 8, 491, doi:10.3390/w8110491, 2016.
- 620 16. Fröhlich C.: *Solar Constant and Total Solar Irradiance Variations*, edited by: Richter, C.,
621 Lincot, D., Gueymard C.A., *Solar Energy*, Springer, New York, NY, 2013.
- 622 17. Gil, L.A., Yaya, O.S., and Shittu, O.I.: Global temperatures and sunspot numbers. Are they
623 related? *Physica A.*, 396, 42–50, 2014.
- 624 18. Gill, A. E.: *Atmosphere–Ocean Dynamics*, International Geophysics Series, Academic Press,
625 edited by: Donn, W. L., 30, 662 pp., eBook ISBN: 9780080570525, Paperback
626 ISBN: 9780122835223, 1982.
- 627 19. Glantz, M. H.: *Once burned, twice shy? Lessons learned from the 1997-1998 El Niño*, The
628 United Nations University, 294 pp, 2001.
- 629 20. Gray, L. J., Beer, J., Geller, M., Haigh, J. D., Lockwood, M., Matthes, K., Cubasch, U.,
630 Fleitmann, D., Harrison, G., Hood, L., Luterbacher, J., Meehl, G. A., Shindell, D., van Geel, B.,
631 and White, W.: Solar influences on climate, *Rev. Geophys.*, 48, RG4001,
632 doi:10.1029/2009RG000282, 2010.

- 633 21. Gray, L. J., Woollings, T. J., Andrews, M., and Knight, J.: Eleven-year solar cycle signal in the
634 NAO and Atlantic/European blocking, *Q. J. Roy. Meteor. Soc.*, 142, 1890–1903,
635 doi:10.1002/qj.2782, 2016.
- 636 22. Hady, Ahmed A.: Deep solar minimum and global climate changes. *J. Advanced Res* (ISSN:
637 2090-1232), Vol: 4, Issue: 3, Page: 209-214. 2013 <https://doi.org/10.1016/j.jare.2012.11.001>.
- 638 23. Haigh, J. D., Winning, A.R., Toumi, R., and Harder, J. W.: An influence of solar spectral
639 variations on radiative forcing of climate, *Nature*, 467, 696–699, 2010.
- 640 24. Harder, J. W., Fontenla, J. M., Pilewskie, P., Richard, E. C., and Woods, T. N.: Trends in solar
641 spectral irradiance variability in the visible and infrared, *J. Geophys. Res. Lett.*, 36L07801,
642 2009.
- 643 25. Hathaway, D. H.: The Solar Cycle, *Living Rev. Sol. Phys.*, 12, 4, doi:10.1007/lrsp-2015-4, 2015.
- 644 26. Hansen J, Kharecha P, Sato M, Masson-Delmotte V, Ackerman F, et al. (2013) Assessing
645 “Dangerous Climate Change”: Required Reduction of Carbon Emissions to Protect Young
646 People, Future Generations and Nature. *PLoS ONE* 8(12): e81648.
647 doi:10.1371/journal.pone.0081648
- 648 27. Henley, B.J., Gergis, J., Karoly, D.J., Power, S., Kennedy, J., and Folland, C.K.: A Tripole Index
649 for the Interdecadal Pacific Oscillation, *Clim. Dynam.*, 45, 3077, doi:10.1007/s00382-015-
650 2525-1, 2015.
- 651 28. Higginson, M. J., M. A. Altabet, L. Wincze, T. D. Herbert, and D. W. Murray (2004), A solar
652 (irradiance) trigger for millennial-scale abrupt changes in the southwest
653 monsoon? *Paleoceanography*, 19, PA3015, doi:10.1029/2004PA001031.
- 654 29. Horning, N., Russell, C., and Goetz, S.: Energy from the Sun to Earth’s Surface. In Chapter 2:
655 Earth’s Radiation Balance and the Global Greenhouse,
656 [https://people.ucsc.edu/~mdmccar/migrated/ocea80b/public/lectures/lect_notes_1/03_En](https://people.ucsc.edu/~mdmccar/migrated/ocea80b/public/lectures/lect_notes_1/03_Energy_Balance_MDM_11F.pdf)
657 [ergy_Balance_MDM_11F.pdf](https://people.ucsc.edu/~mdmccar/migrated/ocea80b/public/lectures/lect_notes_1/03_Energy_Balance_MDM_11F.pdf) (last access: 25 April 2018), 2003.

- 658 30. Huang, B., Banzon, V.F., Freeman, E., Lawrimore, J., Liu, W., Peterson, T.C., Smith, T.M.,
659 Thorne, P. W., Woodruff, S. D., and Zhang, H. M.: Extended Reconstructed Sea Surface
660 Temperature version 4 (ERSST.v4): Part I. Upgrades and intercomparisons, *J. Climate*, 28,
661 911–930, doi:10.1175/JCLI-D-14-00006, 2014.
- 662 31. Huang, B., Thorne, P.W., Banzon, V.F., Boyer, T., Chepurin, G., Lawrimore, J.H., Menne, M.J.,
663 Smith, T. M, Vose, R. S., and Zhang, H. M.: Extended Reconstructed Sea Surface
664 Temperature, Version 5 (ERSSTv5): Upgrades, Validations, and Intercomparisons, *J.*
665 *Climate*, 30, 8179–8205, doi:10.1175/JCLI-D-16-0836.1, 2017.
- 666 32. Huo, W.J., and Xiao, Z.N.: The impact of solar activity on the 2015/16 El Niño event,
667 *Atmospheric and Oceanic Science Letters*, doi: 10.1080/16742834.2016.1231567, 2016.
- 668 33. Ineson, S., Maycock, A. C., Gray, L. J., Scaife, A. A., Dunstone, N. J., Harder, J. W., Knight, J. R.,
669 Lockwood, M., Manners, J. C., and Wood, R. A.: Regional climate impacts of a possible future
670 grand solar minimum, *Nat. Commun.*, 6, 7535, doi:10.1038/ncomms8535, 2015.
- 671 34. Intergovernmental Panel on Climate Change (IPCC) (2001), Third Assessment Report—Climate
672 Change 2001, The Scientific Basis, Cambridge Univ. Press, New York.
- 673 35. Jia, X. and Ge, J. (2017), Modulation of the PDO to the relationship between moderate ENSO
674 events and the winter climate over North America. *Int. J. Climatol*, 37: 4275-4287.
675 doi:10.1002/joc.5083
- 676 36. Knauss, J. A.: Measurements of the Cromwell current, *Deep-Sea Res.*, 6, 265-286,
677 doi.org/10.1016/0146-6313(59)90086-3, 1959.
- 678 37. Kopp, G., and Lean, J. L.: A new, lower value of total solar irradiance: Evidence and climate
679 significance, *J. Geophys. Res. Lett.*, 38L01706, doi:10.1029/2010GL045777, 2011.
- 680 38. Kristoufek, L.: Has global warming modified the relationship between sun spot numbers and
681 global temperatures? *Physica A.*, 468, 351-358, doi: 10.1016/j.physa.2016.10.089, 2017.
- 682 39. Labitzke, K., Austin, J., Butchart, N., Knight J., Takahashi, M., Nakamoto, M., Nagashima, T.,
683 Dorothy, J., and Williams, V.: The global signal of the 11-year solar cycle in the stratosphere:

- 684 Observations and model results, *J. Atmos. Terr. Phys.*, 64, 203-210, doi:10.1016/S1364-
685 6826(01)00084-0, 2002.
- 686 40. Lindsey, R.: Climate and Earth's Energy Budget. In NASA Earth Observatory,
687 <https://earthobservatory.nasa.gov/Features/EnergyBalance/> (last access: 25 April 2018),
688 2009.
- 689 41. Lindsey, R.: In Watching for El Niño and La Niña, NOAA Adapts to Global Warming,
690 [https://www.climate.gov/news-features/understanding-climate/watching-el-ni%C3%B1o-](https://www.climate.gov/news-features/understanding-climate/watching-el-ni%C3%B1o-and-la-ni%C3%B1a-noaa-adapts-global-warming)
691 [and-la-ni%C3%B1a-noaa-adapts-global-warming](https://www.climate.gov/news-features/understanding-climate/watching-el-ni%C3%B1o-and-la-ni%C3%B1a-noaa-adapts-global-warming) (last access: 25 April 2018), 2013.
- 692 42. Liu, F., Chai, J., Huang, G., Liu, J., and Chen, Z.: Modulation of decadal ENSO-like variation by
693 effective solar radiation, *Dynam. Atmos. Oceans*, 72, 52-61, ISSN: 0377-0265, 2015.
- 694 43. Lockwood, M.: Solar change and climate: an update in the light of the current exceptional
695 solar minimum, *P. Roy. Soc. A-Math Phys.*, 466, 303–329, 2010.
- 696 44. Lockwood, M.: Reconstruction and prediction of variations in the open solar magnetic flux
697 and interplanetary conditions, *Living Rev. Sol. Phys.*, 10, 4, 2013.
- 698 45. Maleski, J. J. and Martinez, C. J. (2018), Coupled impacts of ENSO AMO and PDO on
699 temperature and precipitation in the Alabama–Coosa–Tallapoosa and Apalachicola–
700 Chattahoochee–Flint river basins. *Int. J. Climatol*, 38: e717-e728. doi:[10.1002/joc.5401](https://doi.org/10.1002/joc.5401)
- 701 46. Mantua, N. J., Hare, S. R., Zhang, Y., Wallace, J. M., and Francis, R. C.: A Pacific interdecadal
702 climate oscillation with impacts on salmon production, *B. Am. Meteorol. Soc.*, 78, 1069–
703 1079, 1997.
- 704 47. Mantua, N. J., and Hare, S. R.: The Pacific Decadal Oscillation, *J. Oceanogr.*, 58, 35–44, 2002.
- 705 48. McKinley, G. A., Takahashi, T., Buitenhuis, E., Chai, F., Christian, J. R., Doney, S. C., Jiang, M.-
706 S., Lindsay, K., Moore, J.K, Le Quéré, C., Lima, I., Murtugudde, R., Shi, L., and Wetzel, P.:
707 North Pacific carbon cycle response to climate variability on seasonal to decadal timescales,
708 *J. Geophys. Res.*, 111, C07S06, doi:10.1029/2005JC003173, 2006.
-

- 709 49. Montecino, V., and Lange, C. B.: The Humboldt Current System: Ecosystem components and
710 processes, fisheries, and sediment studies, *Prog. Oceanogr.*, 83, 65-79, 2009.
- 711 50. Monteith, J. L.: Solar Radiation and Productivity in Tropical Ecosystems, *J. App. Ecol.*, 9, 747-
712 66, doi:10.2307/2401901, 1972.
-
- 713 51. Montgomery, D. C., Peck, E. A. and Vining, G. G. (2001). *Introduction to Linear Regression*
714 *Analysis*. 3rd Edition, New York, New York: John Wiley & Sons.
- 715 52. Mörner, N.-A.: The Approaching New Grand Solar Minimum and Little Ice Age Climate
716 Conditions, *Natural Science*, 7, 510-518, doi: 10.4236/ns.2015.711052, 2015.
- 717 53. Newman, M., Compo, G. P., and Alexander, M. A.: ENSO-forced variability of the
718 Pacific decadal oscillation, *J. Climate*, 16, 3853-3857, doi: 10.1175/1520-
719 0442(2003)016<3853: EVOTPD>2.0.CO;2., 2003.
- 720 54. Ormaza-González, F.I., and Cedeño, J.: Coastal El Niño 2017 or Simply: The Carnival Coastal
721 Warming Event? *MOJ Ecology & Environmental Sciences*, 2, 00054, doi:
722 10.15406/mojes.2017.02.00054, 2017.
- 723 55. Ormaza-González, F. I., and Sánchez, E.: Cálculo computacional del flujo de energía solar
724 cobre el océano y su aplicación a la zona ecuatorial, *Rev. Ciencias del Mar y Limnología (INP-*
725 *Ecuador)*, 2(1), 27-54, ISSN 1390-5767, 1983.
- 726 56. Ormaza-González, F. I., Mora, A., Bermúdez, R. M., Hurtado, M. A., Peralta, M. R., and
727 Jurado, V. M.: Can small pelagic fish landings be used as predictors to high frequency
728 oceanographic fluctuations in the 1-2 El Niño region? *Adv. Geosci.*, 42, 61–72,
729 doi:10.5194/adgeo-42-61-2016, 2016a.
- 730 57. Ormaza-González, F. I., Mora, A., and Bermúdez, R. M.: Relationships between tuna catch
731 and variable frequency oceanographic conditions, *Adv. Geosci.*, 42, 83–90,
732 doi:10.5194/adgeo-42-83-2016, 2016b.

- 733 58. Ramírez, I.J. & Briones, Understanding the El Niño Costero of 2017: The Definition Problem
734 and Challenges of Climate Forecasting and Disaster Responses, *F. Int J Disaster Risk Sci* 8:
735 489. <https://doi.org/10.1007/s13753-017-0151-8>, 2017.
- 736 1. Rasmussen, E. M., and Carpenter, T. H.: Variations in tropical sea surface temperature and
737 surface wind fields associated with the Southern Oscillation/El Niño, *Mon. Weather*
738 *Rev.*, 110, 354-384, 1982.
- 739 2. Scafetta, N.: Global temperatures and sun spot numbers. Are they related? Yes, but non-
740 linearly. A reply to Gil-Alana et al. (2014), *Physica A.*, 413, 329-342, doi:
741 10.1016/j.physa.2014.06.047, 2014.
- 742 3. Shindell, D. T., Schmidt, G. A., Mann, M. E., Rind, D., and Waple, A.: Solar Forcing of Regional
743 Climate Change During the Maunder Minimum, *Science*, 294 (5549), 2149-2152, doi:
744 10.1126/science.1064363, 2001.
- 745 4. Schlesinger, M. E., and Ramankutty, N.: An oscillation in the global climate system of period
746 65–70 years, *Nature*, 367, 723–726, doi:10.1038/367723a0., 1994.
- 747 5. Smyth, T. J. 2011. Penetration of UV irradiance into the global ocean. *J. Geophys.*
748 *Res.*, 116C11020, doi:10.1029/2011JC007183.
- 749 6. Trenberth, K.E., Fasullo, J.T., and Balmaseda, M.A.: Earth’s Energy Imbalance, *J. Climate*, 27,
750 3129–3144, doi:10.1175/JCLI-D-13-00294.1, 2014.
- 751 7. van Oldenborgh, G. J., te Raa, L. A., Dijkstra, H. A., and Philip, S. Y.: Frequency- or amplitude-
752 dependent effects of the Atlantic meridional overturning on the tropical Pacific Ocean,
753 *Ocean Sci.*, 5, 293-301, doi:10.5194/os-5-293-2009, 2009.
- 754 8. van Loon, H., Meehl, G. A., and Shea, D. J.: Coupled air-sea response to solar forcing in the
755 Pacific region during northern winter, *J. Geophys. Res.*, 112D02108,
756 doi:10.1029/2006JD007378, 2007.

- 757 9. Wang, G., Cheng, L., Abraham, J., and Li, C.: Consensuses and discrepancies of basin-scale
758 ocean heat content changes in different ocean analyses, *Clim. Dynam.*, doi:10.1007/s00382-
759 017-3751-5, 2017.
- 760 10. Wenjuan, H., and XIAO, Z.: The impact of solar activity on the 2015/16 El Niño event,
761 *Atmospheric and Oceanic Science Letters*, doi:10.1080/16742834.2016.1231567, 2016.
- 762 11. White, W. B., Lean, J., Cayan, D. R., and Dettinger, M. D.: Response of global upper ocean
763 temperature to changing solar irradiance, *J. Geophys. Res.*, 102(C2), 3255–3266,
764 doi:10.1029/96JC03549, 1997.
- 765 12. Wolter, K., and Timlin, M.S.: Monitoring ENSO in COADS with a seasonally adjusted principal
766 component index, *Proceedings of the 17th Climate Diagnostics Workshop*, 52-57, Norman,
767 OK, 1993.
- 768 13. Wolter, K., and Timlin, M. S.: Measuring the strength of ENSO events - how does 1997/98
769 rank? *Weather*, 53, 315-324, 1998.
- 770 14. Wolter, K., and Timlin, M. S.: El Niño/Southern Oscillation behaviour since 1871 as diagnosed
771 in an extended multivariate ENSO index (MEI.ext), *Int. J. Climatol.*, 31, 1074–1087,
772 doi:10.1002/joc.2336, 2011.
- 773 15. Yamakawa, S., Makoto, I., and Ramasamy, S.: Relationships between solar activity and
774 variations in SST and atmospheric circulation in the stratosphere and troposphere, *Quatern.*
775 *Int.*, 397, 289-299, 2016.
- 776 16. Yim, B. Y., Noh, Y., Yeh, S. -W., Kug, J. -S., Min, H. S., and Qiu, B.: Ocean mixed layer
777 processes in the Pacific Decadal Oscillation in coupled general circulation models, *Clim.*
778 *Dynam*, 41, 1407–1417, doi: 10.1007/s00382-012-1630-7, 2013.
- 779 17. Yoon, J., and Yeh, S. -W.: Influence of the Pacific Decadal Oscillation on the Relationship
780 between El Niño and the Northeast Asian Summer Monsoon, *J. Climate*, 23, 4525–4537,
781 doi:10.1175/2010JCLI3352.1, 2010.

- 782 18. Yuan, Y., and Yan, H.: Different types of La Niña events and different responses of the
783 tropical atmosphere, *Chinese Sci. Bull.*, 58, 406–415, doi:10.1007/s11434-012-5423-5, 2012.
- 784 19. Zhang, Y., Wallace, J. M., and Battisti, D. S.: ENSO-like Interdecadal Variability: 1900–93, *J.*
785 *Climate*, 10, 1004-1020, 1997.
- 786 20. Zheng, F., Fang, X.-H., Zhu, J., Yu, J.-Y., and Li, X.-C.: Modulation of Bjerknes feedback on the
787 decadal variations in ENSO predictability, *J. Geophys. Res. Lett.*, 43, 560–568,
788 doi:10.1002/2016GL07163, 2016.
- 789 21. Zhou, J., and Tung, K. -K.: Solar Cycles in 150 Years of Global Sea Surface Temperature Data,
790 *J. Climate*, 23, 3234-3248, 2010.
- 791 22. Zong, Z., Yong, L., and Jian, H.: Effects of Sunspot on the Multi-Decadal Climate Projections,
792 *Advances in Climate Change Research*, 5, 51-56, doi:10.3724/SP.J.1248.2014.051, 2014.
- 793

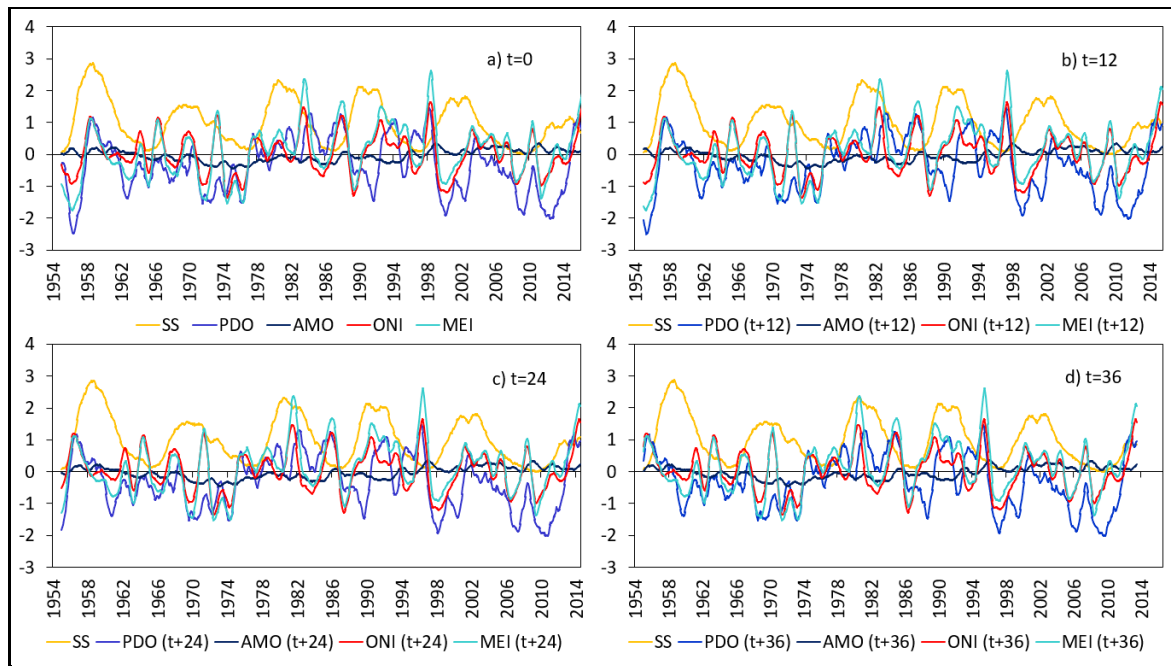
794

795 **Table 1.** Linear correlations (r^2 and p-values) between SS monthly counts and PDO, MEI, ONI, AMO,
 796 SST and SST Anomaly in 1+2, and 3.4 for the period April 1954 to December 2017. Negative r^2 means
 797 negative slopes of the linear regression curves.

Variable		(t+0)	(t+6)	(t+12)	(t+24)	(t+36)	(t+48)
PDO	r^2	0.00	0.02	0.04	0.04	0.03	0.02
	p-value	3.83E-01	1.75E-04	1.94E-07	1.26E-08	2.07E-06	3.11E-05
MEI	r^2	0.01	0.02	0.03	0.02	0.01	0.00
	p-value	2.58E-02	9.68E-05	2.55E-06	1.63E-05	1.51E-02	9.30E-01
ONI	r^2	0.01	0.03	0.04	0.03	0.01	0.00
	p-value	2.22E-03	4.93E-06	2.11E-07	1.91E-06	4.00E-03	4.13E-01
AMO	r^2	0.00	-8.30E-04	-9.66E-04	-2.89E-03	0.01	0.02
	p-value	7.97E-01	4.28E-01	3.94E-01	1.44E-01	1.45E-03	2.21E-04
SST 1+2	r^2	-2.54E-04	1.61E-03	-3.08E-05	-2.92E-06	-3.04E-04	-1.26E-03
	p-value	6.61E-01	2.71E-01	8.80E-01	9.63E-01	6.37E-01	3.44E-01
SSTA 1+2	r^2	0.00	0.00	0.00	0.00	0.00	-0.00
	p-value	7.14E-01	1.67E-01	3.37E-01	2.57E-01	8.13E-01	3.73E-01
SST 3.4	r^2	0.00	0.01	0.01	0.01	0.00	-0.00
	p-value	2.78E-01	5.93E-03	1.07E-03	1.32E-03	6.48E-02	9.10E-01
SSTA 3.4	r^2	0.00	0.01	0.02	0.02	0.01	0.00
	p-value	1.45E-01	2.25E-03	8.23E-05	1.23E-04	2.45E-02	9.79E-01

798

799 **Fig. 1.** Behaviour of monthly counts of SS, ONI, MEI, PDO and AMO. The indexes start at t= 0, 12, 24
 800 and 36 months (panels a, b, c and d respectively). The SS series starts at t=0 in the four panels. The
 801 vertical axis gives the values for the indexes and SS numbers (multiply by 100).

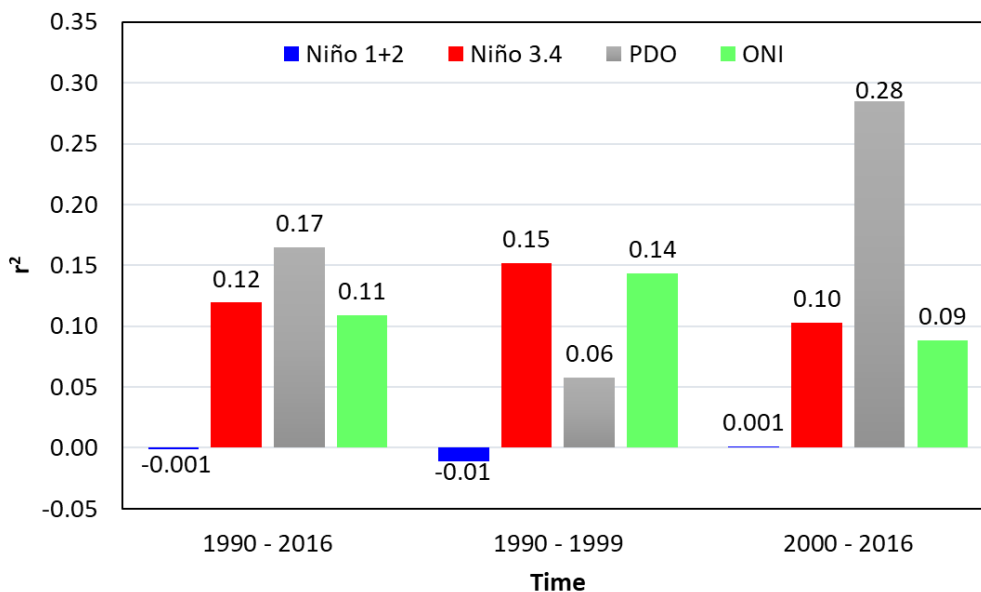


802

803

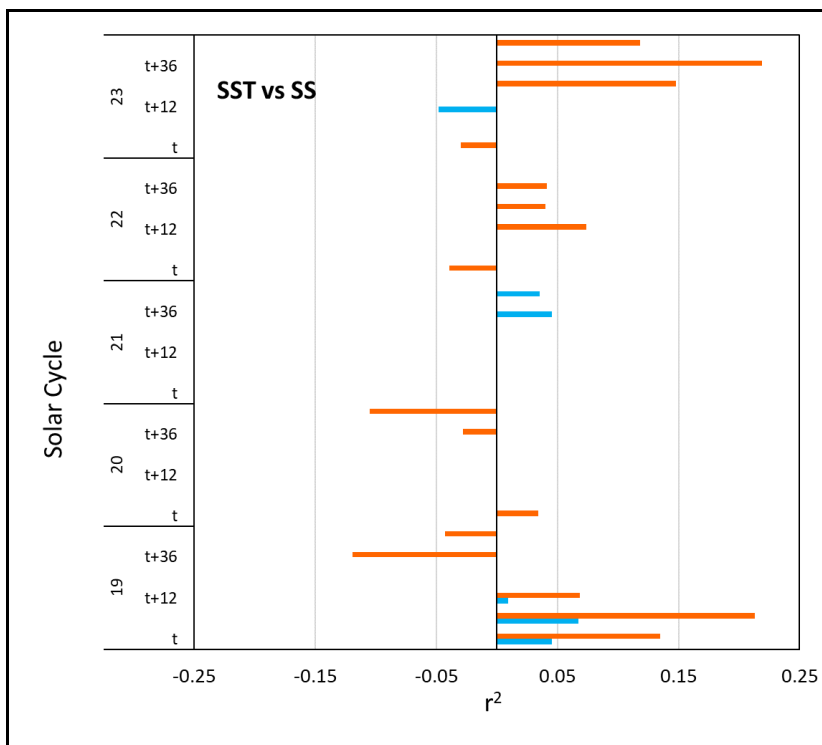
804

805 **Fig. 2.** Linear regression correlation coefficient r^2 ($p < 0.05$) of SS monthly counts against SST Anomaly
 806 in regions El Niño 1+2 (blue) and 3.4 (red) and indexes PDO (grey) and ONI (green) through three
 807 time periods.



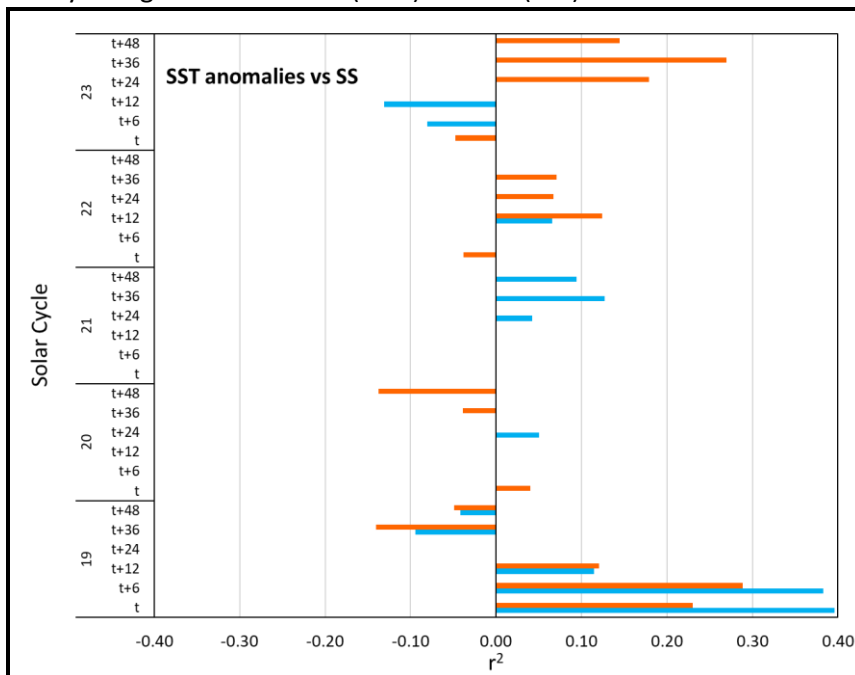
808

809 **Fig. 3.** Linear regression correlation coefficient r^2 ($p < 0.05$) of SS monthly counts for cycles 19-24
 810 against SST in regions El Niño 1+2 (blue) and 3.4 (red).



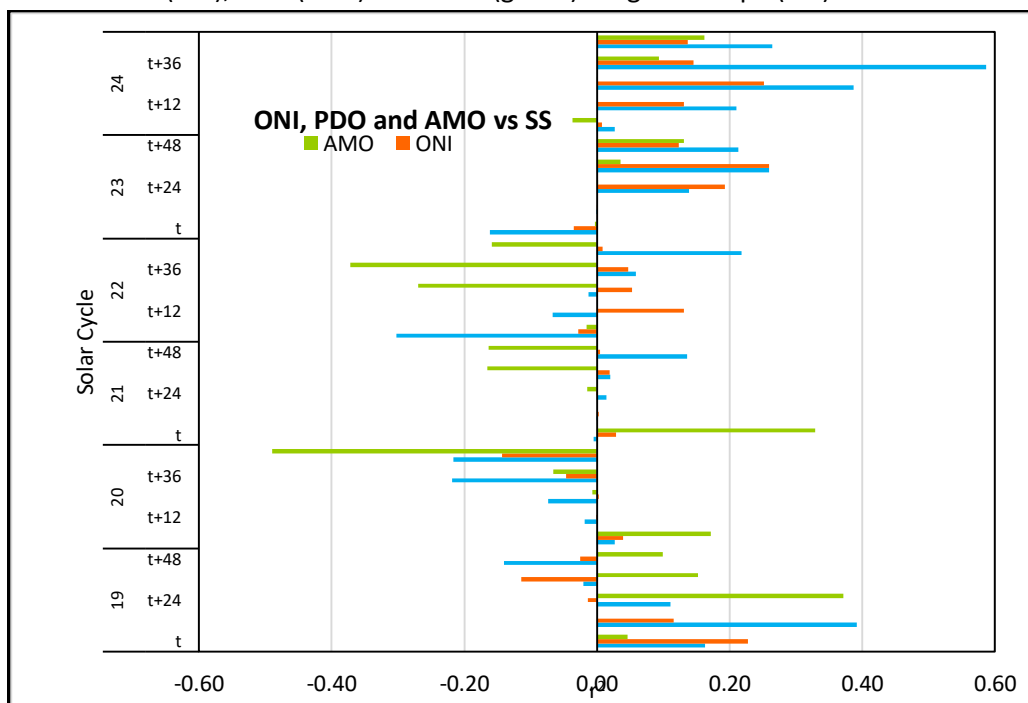
811

812 **Fig. 4.** Linear regression correlation coefficient r^2 ($p < 0.05$) of SS monthly counts of cycles 19-24
 813 against SST Anomaly in regions El Niño 1+2 (blue) and 3.4 (red).



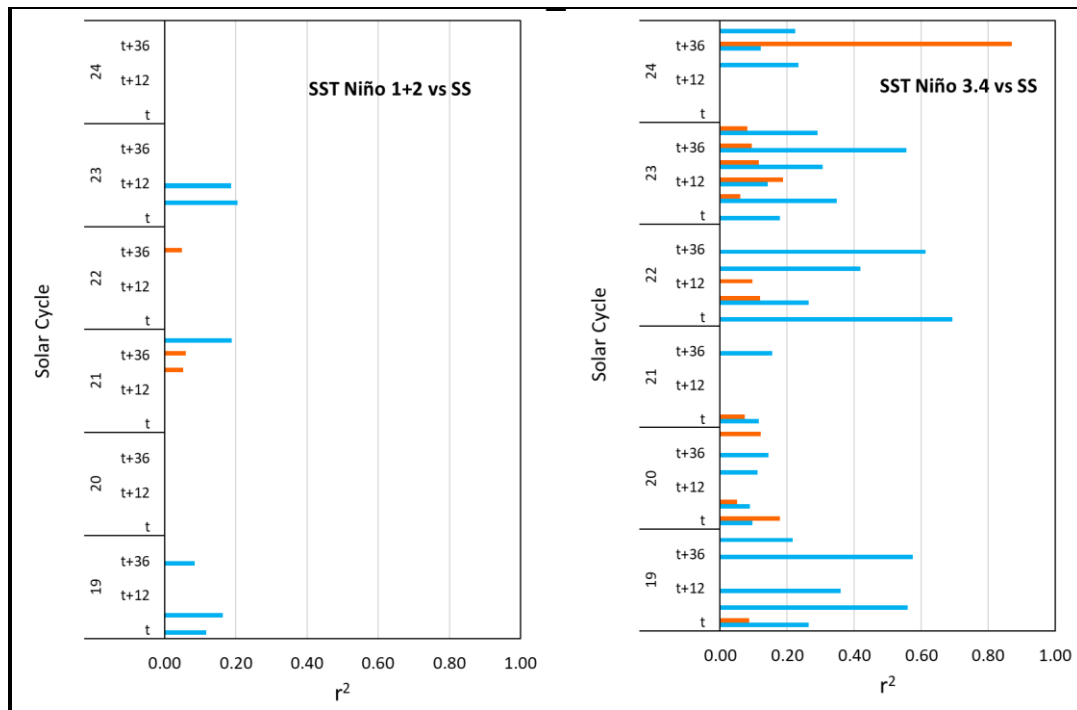
814
 815
 816

817 **Fig. 5.** Linear regression correlation coefficient r^2 ($p < 0.05$) of SS monthly counts cycles 19-24 against
 818 indexes: ONI (red), PDO (blue) and AMO (green). Negative slope ($-r^2$).

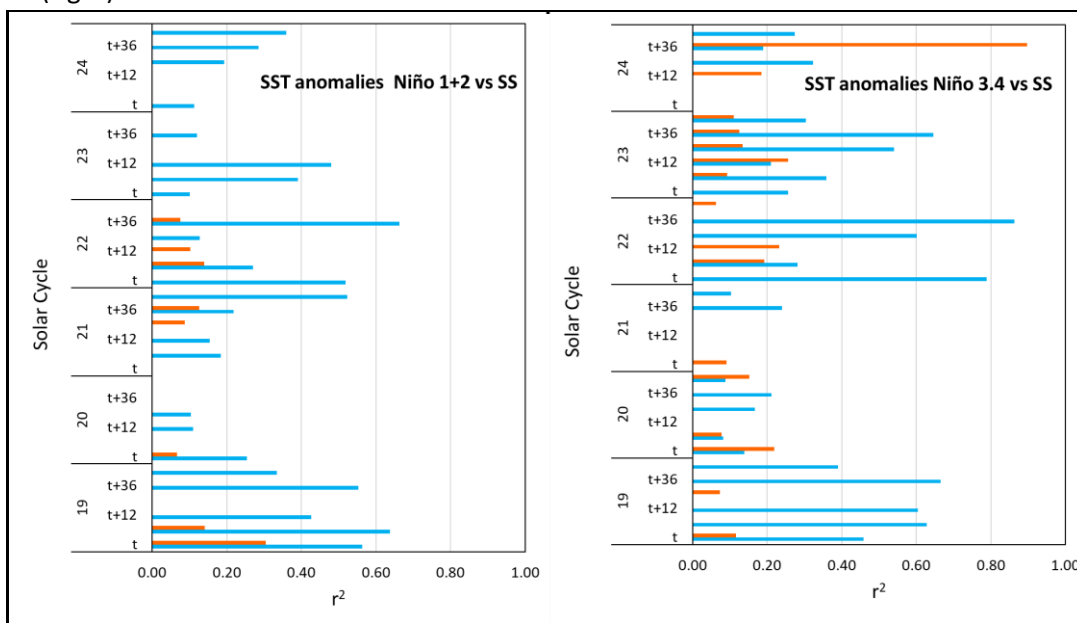


819
 820

821 **Fig. 6.** Linear regression correlation coefficient r^2 ($p < 0.05$) of SS monthly counts during the ascending
 822 (blue) and descending (red) phases of SS for cycles 19-24 against SST in regions El Niño 1+2 (left) and
 823 3.4 (right).

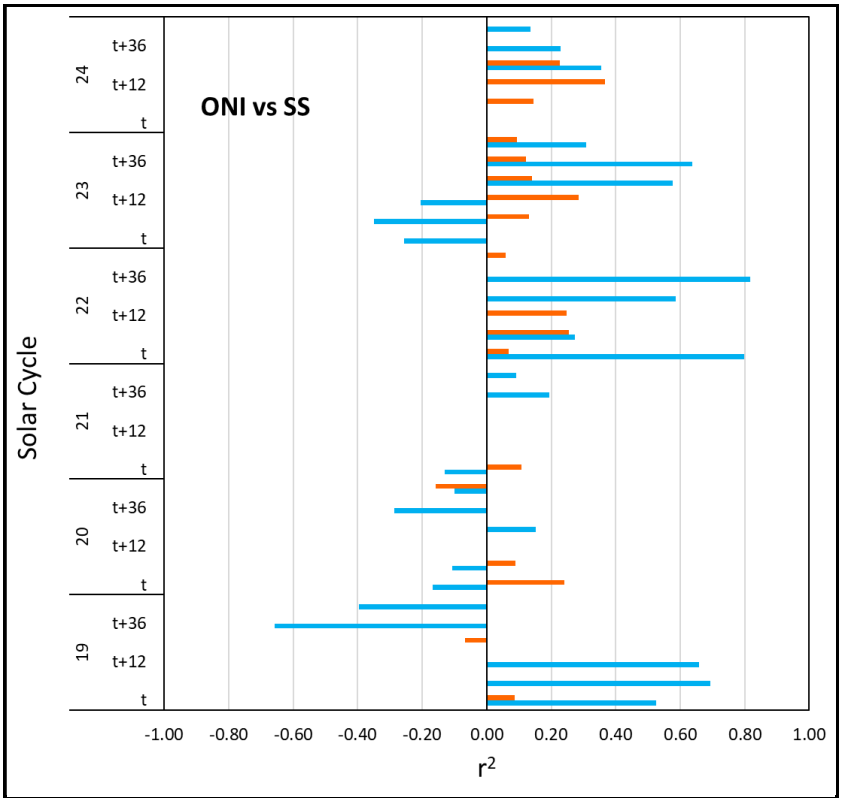


824
 825
 826 **Fig. 7.** Linear regression correlation coefficient r^2 ($p < 0.05$) of SS monthly counts during the ascending
 827 (blue) and declining (red) phases for SS cycles 19-24 against SST Anomaly in regions El Niño 1+2 (left)
 828 and 3.4 (right).



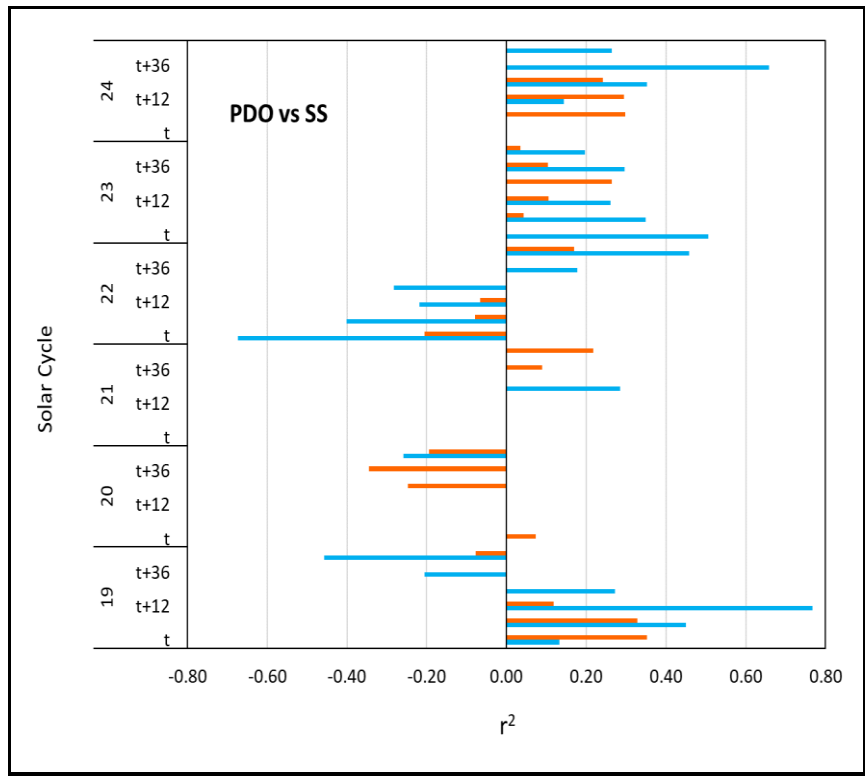
829
 830

831 **Fig. 8.** Linear regression correlation coefficient r^2 of SS monthly counts during the ascending (blue)
 832 and declining (red) phases of SS cycles (19-24) against index ONI. Negative slope ($-r^2$).



833
 834
 835
 836
 837

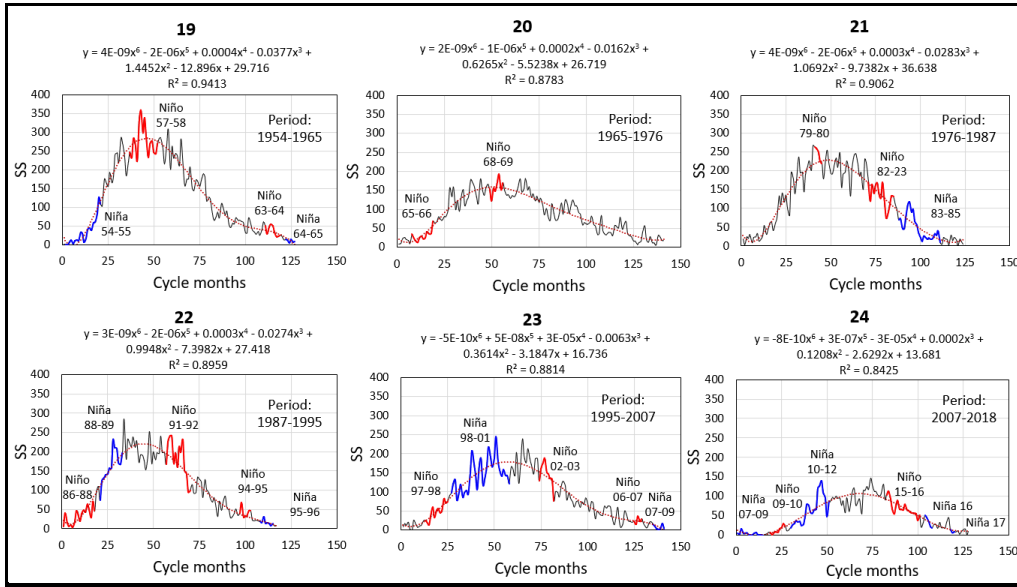
Fig. 9. Linear regression correlation coefficient r^2 ($p < 0.05$) of SS monthly counts during the ascending (blue) and declining (red) phases of SS cycles (19-24) against index PDO. Negative slope ($-r^2$).



838

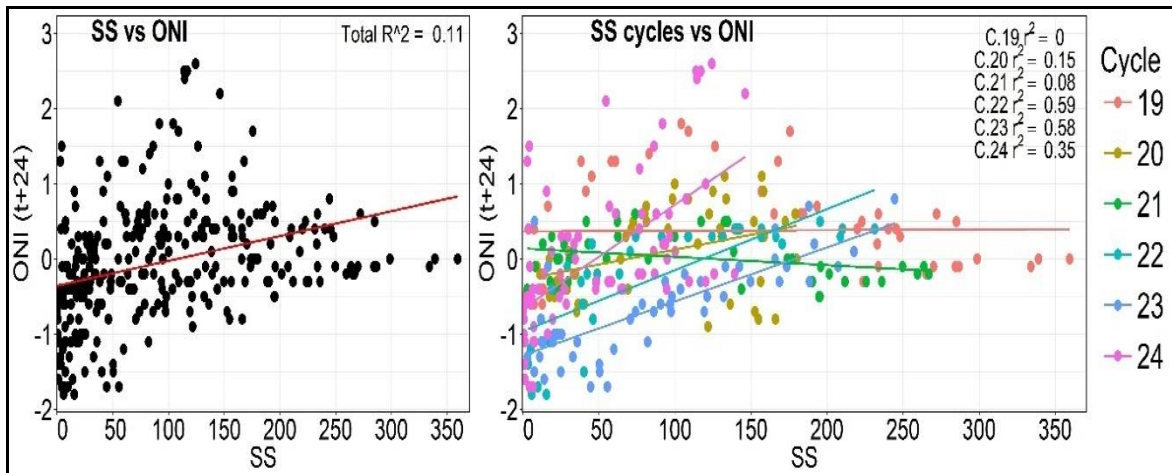
839
840
841

Fig. 10. Polynomial functions of 6 degrees ($p < 0.001$), based on monthly SS counts. Red and blue lines represent El Niño and La Niña event. The cycle number of the top of each panel.



842
843

Fig. 11. Linear regression curves for all ascendants phases of cycles 19-24 (left panel) and per each cycle (right panel).



846